

PLANETARY SCIENCE

Clay mineral diversity and abundance in sedimentary rocks of Gale crater, Mars

Thomas F. Bristow^{1*}, Elizabeth B. Rampe^{2*}, Cherie N. Achilles³, David F. Blake¹, Steve J. Chipera⁴, Patricia Craig⁵, Joy A. Crisp⁶, David J. Des Marais¹, Robert T. Downs³, Ralf Gellert⁷, John P. Grotzinger⁸, Sanjeev Gupta⁹, Robert M. Hazen¹⁰, Briony Horgan¹¹, Joanna V. Hogancamp², Nicolas Mangold¹², Paul R. Mahaffy¹³, Amy C. McAdam¹³, Doug W. Ming², John Michael Morookian⁶, Richard V. Morris², Shaunna M. Morrison¹⁰, Allan H. Treiman⁵, David T. Vaniman¹⁴, Ashwin R. Vasavada⁶, Albert S. Yen⁶

Copyright © 2018
The Authors, some
rights reserved;
exclusive licensee
American Association
for the Advancement
of Science. No claim to
original U.S. Government
Works. Distributed
under a Creative
Commons Attribution
NonCommercial
License 4.0 (CC BY-NC).

Clay minerals provide indicators of the evolution of aqueous conditions and possible habitats for life on ancient Mars. Analyses by the Mars Science Laboratory rover Curiosity show that ~3.5-billion year (Ga) fluvio-lacustrine mudstones in Gale crater contain up to ~28 weight % (wt %) clay minerals. We demonstrate that the species of clay minerals deduced from x-ray diffraction and evolved gas analysis show a strong paleoenvironmental dependency. While perennial lake mudstones are characterized by Fe-saponite, we find that stratigraphic intervals associated with episodic lake drying contain Al-rich, Fe³⁺-bearing dioctahedral smectite, with minor (3 wt %) quantities of ferripyrophyllite, interpreted as wind-blown detritus, found in candidate aeolian deposits. Our results suggest that dioctahedral smectite formed via near-surface chemical weathering driven by fluctuations in lake level and atmospheric infiltration, a process leading to the redistribution of nutrients and potentially influencing the cycling of gases that help regulate climate.

INTRODUCTION

The Mars Science Laboratory (MSL) rover Curiosity has documented sedimentary rocks on the floor of Gale crater and the lower slopes of the crater's central mound, Aeolis Mons (informally known as Mt. Sharp), since landing in August 2012 (1, 2). Early in the mission, at Yellowknife Bay (YKB) (1), lacustrine mudstones of the Sheepbed member were shown to contain ~20 weight % (wt %) clay mineral, which was identified as Fe-rich saponite. Saponite was proposed as forming close to the time of sediment deposition by isochemical aqueous alteration of detrital olivine under anoxic to poorly oxidizing conditions (3–5). By providing constraints on pH and possible substrates for chemolithoautotrophs during deposition, the clay minerals are key indicators of an ancient habitable lake (1, 3, 4). D/H ratios of clay minerals combined with their mode of formation also constrain the global inventory of martian water ~3.5 billion years (Ga) ago (6).

YKB gave an early glimpse of part of a spatially and temporally extensive Early Hesperian (~3.5 Ga) fluvial-lacustrine system that likely occupied much of Gale crater, which MSL continues to explore as part of its now >18-km traverse of the crater floor and lower slopes

of Mt. Sharp (2). Mineralogical and geochemical investigations of these sediments have revealed the dynamic natures of lake water chemistry and early diagenetic conditions, with evidence of redox stratification in the lake and/or variations in pH and E_h during subsequent diagenesis (7, 8). Clay minerals were found in sandstones and mudstone samples stratigraphically above YKB at Windjana in the Kimberley formation, and in various samples of the Murray formation outcrops in the Pahrump Hills (Figs. 1 and 2) (7, 9, 10). The identified clay minerals largely belong to the 2:1 group (7, 9), a family of phyllosilicates with a diverse range of physical, chemical, and crystallographic properties (11–13). However, their low abundance (~10 wt % or less), combined with x-ray diffraction (XRD) peak overlap from co-occurring pyroxene minerals (7, 9, 10), prevents detailed crystallography and chemical characterization. As a result, key constraints on the origin and genesis of clay minerals are not accessible. Here, we provide these details for clay minerals in the four most recent drill samples of Murray formation mudstones, stratigraphically above the basal Pahrump Hills member (Fig. 1).

RESULTS

The four Murray formation samples we investigated are drill powders, collected from a depth of 5 to 6 cm in the bedrock, by Curiosity's Sample Acquisition, Processing, and Handling (SA/SPaH). The samples in stratigraphic order, shown in Fig. 1, are as follows: Oudam, from a ~25-m-thick unit of cross-stratified siltstones and very fine-grained sandstones of the Hartmann's Valley member, likely aeolian in origin, although a fluvial interpretation has been discussed; Marimba and Quela, which come from a ~30-m-thick package of finely laminated mudstones of the Karasburg member, representing a return to subaqueous deposition; and Sebina, from the Sutton Island member that consists of heterolithic mudstone-sandstones containing desiccation cracks and other sedimentary structures, suggesting episodic drying and subaerial exposure of the Gale lake (14–16). By examining the clay mineralogy of samples in their geological context, we constrain the timing,

¹NASA Ames Research Center, Moffett Field, CA 94035, USA. ²NASA Johnson Space Center, Houston, TX 77058, USA. ³Department of Geosciences, University of Arizona, Tucson, AZ 85721, USA. ⁴Chesapeake Energy, Oklahoma City, OK 73154, USA. ⁵Lunar and Planetary Institute, Houston, TX 77058, USA. ⁶Jet Propulsion Laboratory, California Institute of Technology, Pasadena, CA 91109, USA. ⁷Department of Physics, University of Guelph, Guelph, Ontario N1G 2W1, Canada. ⁸Division of Geologic and Planetary Sciences, California Institute of Technology, Pasadena, CA 91125, USA. ⁹Department of Earth Science and Engineering, Imperial College London, London SW7 2AZ, UK. ¹⁰Geophysical Laboratory, Carnegie Institution of Washington, Washington, DC 20015, USA. ¹¹Earth, Atmospheric, and Planetary Sciences Department, Purdue University, West Lafayette, IN 47907, USA. ¹²Laboratoire de Planétologie et Géodynamique, UMR6112, CNRS, Université Nantes, Université Angers, Nantes, France. ¹³NASA Goddard Space Flight Center, Greenbelt, MD 20771, USA. ¹⁴Planetary Science Institute, Tucson, AZ 85719, USA.

*Corresponding author. Email: thomas.f.bristow@nasa.gov (T.F.B.); elizabeth.b.rampe@nasa.gov (E.B.R.)

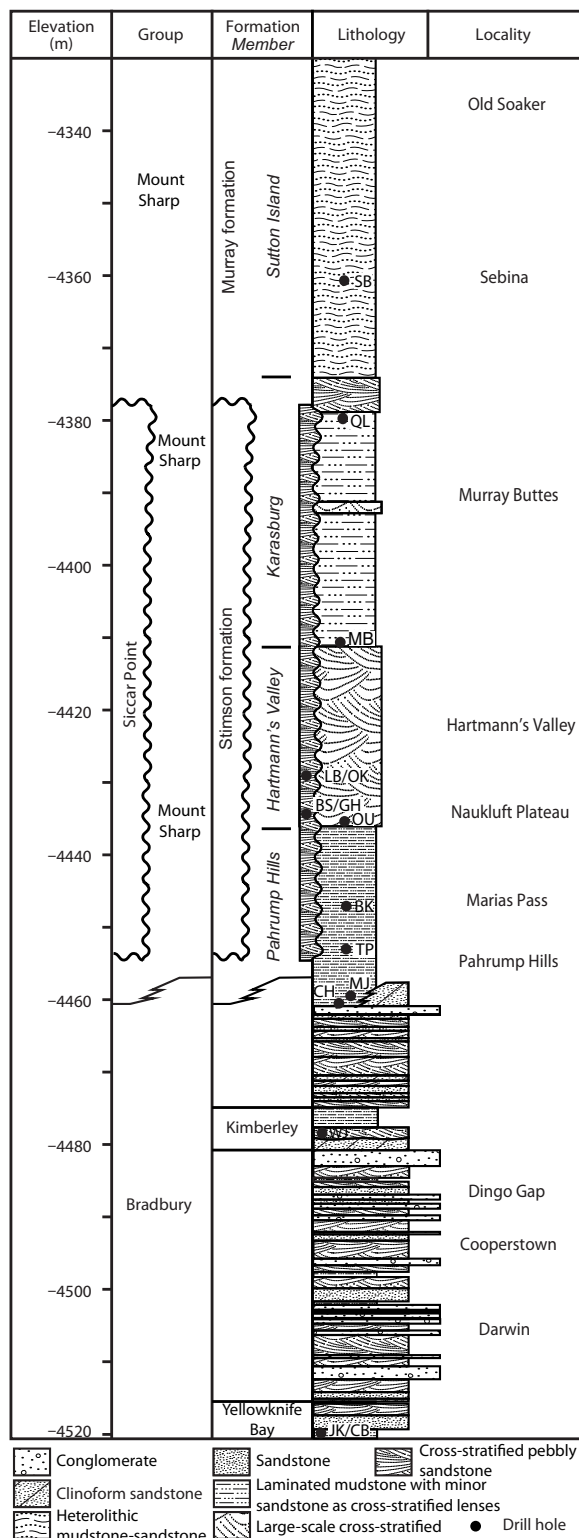


Fig. 1. Stratigraphic column of sedimentary rocks at Gale crater observed by MSL, showing positions of drill samples. The stratigraphic framework of Gale crater sediments shown here was established by Grotzinger *et al.* (2) and is actively updated and refined through the efforts of the MSL sedimentology/stratigraphy working group (14). SB, Sebina; QL, Quela; MB, Marimba; OU, Oudam; BK, Buckskin; TP, Telegraph Peak; MJ, Mojave2; CH, Confidence Hills; WJ, Windjana; JK/CB, John Klein/Cumberland.

locus, and mechanisms of the clay mineral formation. Our findings are relevant to debates concerning surficial versus crustal origins of clay minerals detected from orbit, which have implications for the planetary hydrology and climate of early Mars (17–19).

CheMin XRD analysis (Materials and Methods) shows that clay minerals make up ~15 to 28 wt % of the bulk rock, with similar contributions to XRD patterns in Marimba, Quela, and Sebina (Table 1). As observed in nearly every clay mineral-bearing sample collected by MSL (Oudam is the exception, as described below), broad basal reflections at $\sim 10^\circ 2\theta$ Co K α (~ 10 Å) indicate the presence of 2:1 group clay minerals (Fig. 3A). The 02 l clay mineral band, which is sensitive to the occupancy and species of cations within the octahedral sheets of clay minerals (20), peaks at $\sim 22.9^\circ 2\theta$ Co K α (4.50 Å; Fig. 3B). This band position is characteristic of dioctahedral 2:1 clay minerals (13, 20). Trioctahedral smectites in YKB samples (John Klein and Cumberland) have a distinctly different 02 l band position ($\sim 22.7^\circ 2\theta$, 4.58 Å) (Fig. 3B) (3, 4).

The CheMin sample cells maintain near-constant, very low humidity, which would promote loss of interlayer H₂O and collapse of smectite interlayers, making them difficult to distinguish from illite based on basal reflection position alone (3, 4). However, illite, which typically contains fixed K in the interlayer (4, 11–13), does not appear to be a significant component of these samples based on the lack of correlation between clay content of Murray formation mudstones and K content of the bulk samples (fig. S1). Smectitic clay minerals appear to be most abundant, with the K contents of samples accounted for by sanidine, jarosite, and x-ray amorphous material (table S1) (10).

SAM (Sample Analysis at Mars) evolved gas analyses (EGAs; see Materials and Methods) give additional information on the nature of the octahedral sheets of the Murray clay minerals. The temperature of H₂O loss during heat-driven dehydroxylation of clay minerals is sensitive to cation content, occupancy, and the position of the vacant octahedral sites in dioctahedral clay minerals (21–23). Peak H₂O release of the Marimba sample occurred at 610° and 780°C, indicating the presence of both dioctahedral and trioctahedral components, respectively (Fig. 4) (21–24). EGA data are inconsistent with the most Fe(III)-rich dioctahedral smectites such as nontronite, which have diagnostic dehydroxylation temperatures of <550°C (21–24). Comparison of the dioctahedral-assigned EGA peak at 610°C with laboratory studies of dehydroxylation temperature systematics as a function of Fe content suggests that the dioctahedral smectite likely contains ~5 wt % Fe₂O₃, requiring that at least half of octahedral sites are occupied by Al (25). The peak water release at 780°C, assigned to Mg-rich trioctahedral smectite, is higher than the 725°C peak observed for YKB samples (24), indicating that trioctahedral smectites in Marimba have a comparatively lower Fe content.

These observations are consistent with the CheMin XRD analyses. The position of the 02 l clay mineral band is best modeled when measured clay mineral standards or structural models of both trioctahedral and Al-rich dioctahedral smectites are used in Rietveld refinements of the XRD patterns (Fig. 3C; Materials and Methods). On the basis of the combination of XRD, EGA, and bulk chemical data measured by the alpha particle x-ray spectrometer (APXS), we find that a mixture of Al-rich dioctahedral and Mg-rich trioctahedral smectite is present in Marimba, Quela, and Sebina. This is the first in situ detection of dioctahedral smectite in Gale crater.

There have been no direct orbital detections of phyllosilicate in strata traversed (so far) by Curiosity. Recent orbital visible and near-infrared (VNIR) spectra have documented signatures of Al/Fe-smectites in laterally (and presumably time equivalent) units of the Karasburg and

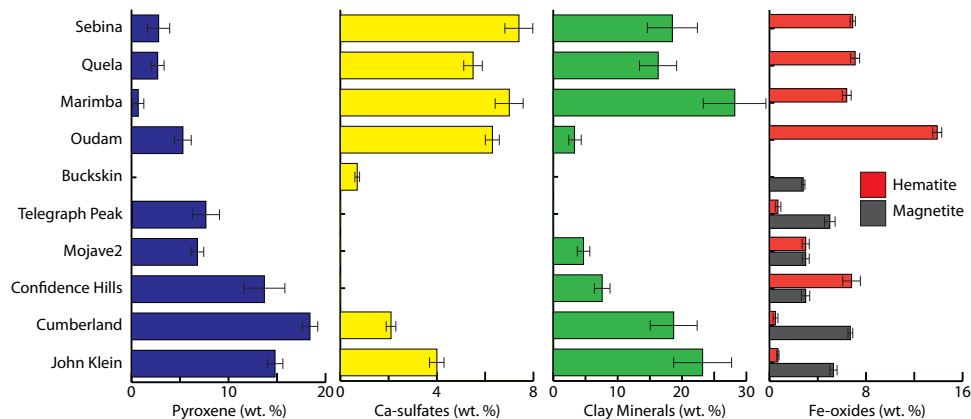


Fig. 2. Changes in abundances of environmentally sensitive mineralogical components in mudstones along MSLs' traverse. Samples are arranged in stratigraphic order. Mineral abundances and associated 1σ errors shown for John Klein and Cumberland, Confidence Hills to Buckskin, and Oudam to Sebina are sourced from Morrison *et al.* (10), Rampe *et al.* (7), and Table 1, respectively.

Table 1. Mineralogical composition (wt %) of Oudam, Marimba, Quela, and Sebina with 1σ errors. Detection limits for crystalline materials are 0.5 wt %.

Mineral	Oudam	Marimba	Quela	Sebina
Andesine	27.8 ± 0.5	14.0 ± 0.9	13.5 ± 0.7	10.7 ± 0.4
Hematite	13.9 ± 0.4	6.4 ± 0.4	7.1 ± 0.4	6.9 ± 0.2
Ca-sulfate	6.3 ± 0.3	7.0 ± 0.6	5.5 ± 0.4	7.4 ± 0.6
Sanidine	—	2.4 ± 0.6	2.3 ± 0.5	1.4 ± 0.4
Pyroxene	5.3 ± 0.9	0.7 ± 0.6	2.7 ± 0.7	2.8 ± 0.4
Jarosite	—	At detection	At detection	0.9 ± 0.2
Quartz	0.7 ± 0.1	At detection	At detection	At detection
Clay minerals	3 ± 1	28 ± 5	16 ± 3	19 ± 4
Amorphous	43 ± 20	40 ± 20	52 ± 25	51 ± 25

Sutton Island members of the Murray formation (fig. S2) (26, 27). Our rover-based results presented here are the first crystallographic ground truth of the thousands of orbital phyllosilicate detections, which are essential inputs for Mars science and mission planning (17–19). Our results confirm the presence of Al-rich dioctahedral smectite (co-occurring with trioctahedral smectite) and other mineralogical information that helps constrain the origin and environmental implications of these clay minerals.

By incorporating structural models of clay minerals, with the *b*-unit cell parameter constrained by dehydroxylation temperatures observed in Marimba, Rietveld refinements of XRD patterns provide an estimate of the ratio of dioctahedral to trioctahedral smectites (Materials and Methods). The proportion of dioctahedral smectite increases up-section, with dioctahedral/trioctahedral ratios of 1:2, 1:1, and 5:3 for Marimba, Quela, and Sebina, respectively. The formation of Al-bearing dioctahedral smectites from basaltic precursors requires greater element mobility and more oxidizing conditions than the suboxic, isochemical aqueous alteration environments proposed for the Fe-saponite of YKB (3, 4). For example, in terrestrial weathering profiles of basaltic rocks, the initial alteration products of olivine typically contain trioctahedral smectite

species with compositions (for example, Mg/Fe) related to those of the primary minerals (13). As alteration progresses, trioctahedral smectites are replaced by dioctahedral clay minerals via removal of Fe^{2+} and Mg^{2+} and/or oxidation of Fe^{2+} and passive enrichment of Si and Al (11–13). Oxidizing conditions also tend to lower pH, which is less favorable for the formation of Mg-trioctahedral clay minerals (28). As a consequence, trioctahedral smectites are rarely found in basaltic soils.

The formation of dioctahedral smectite is not restricted to surface weathering profiles; on a basaltic planet like Mars, dioctahedral smectites could form in a variety of surface and subsurface aqueous environments (17–19, 28). Several observations indicate that the smectitic clay minerals in Marimba, Quela, and Sebina were subject to modification or formed close to the time of deposition within the Gale sedimentary system. There is no evidence from orbital VNIR spectra for Al-bearing clay minerals in the rim and walls of Gale crater, suggesting that the clay minerals we describe were not sourced there (29). The accompanying trends in sedimentary facies, as well as bulk mineralogy and geochemistry of mudstones, indicate that the occurrence of Al-bearing, dioctahedral smectite corresponds with a shift in environmental conditions and the degree of chemical alteration in Gale crater lake sediments. Figure 2 shows the changes in abundances of environmentally sensitive mineral components along MSL's traverse, including (i) a transition from magnetite to hematite as the main Fe-oxide; (ii) an increase in the abundances of Ca-sulfates, which appear to be matrix components above the Pahrump Hills member of the Murray formation and thus indicators of near-surface evaporative processes; and (iii) an overall reduction in the quantity of reactive mafic minerals—pyroxene and olivine. These mineralogical trends broadly correspond with observed sedimentary indicators of shallowing and episodic lake desiccation (14, 16). The observed increase in the degree of aqueous alteration of mafic detritus in the upper part of the Murray formation is also reflected in chemical indices of alteration derived from bulk geochemical analyses (30).

Our preferred mechanism for the production of Murray dioctahedral smectites involves open-system aqueous alteration of basaltic detritus in the lake, near the time of deposition, with elemental mobilization and oxidation driven by periodic desiccation and migration of the water table. Trioctahedral smectites may be the remnants of early-stage alteration of olivine or pyroxene, as proposed for YKB (2–5), or the product of high Mg^{2+} activities in lake water and sedimentary pore water caused by evaporation (31). Higher dehydroxylation temperatures indicate elevated

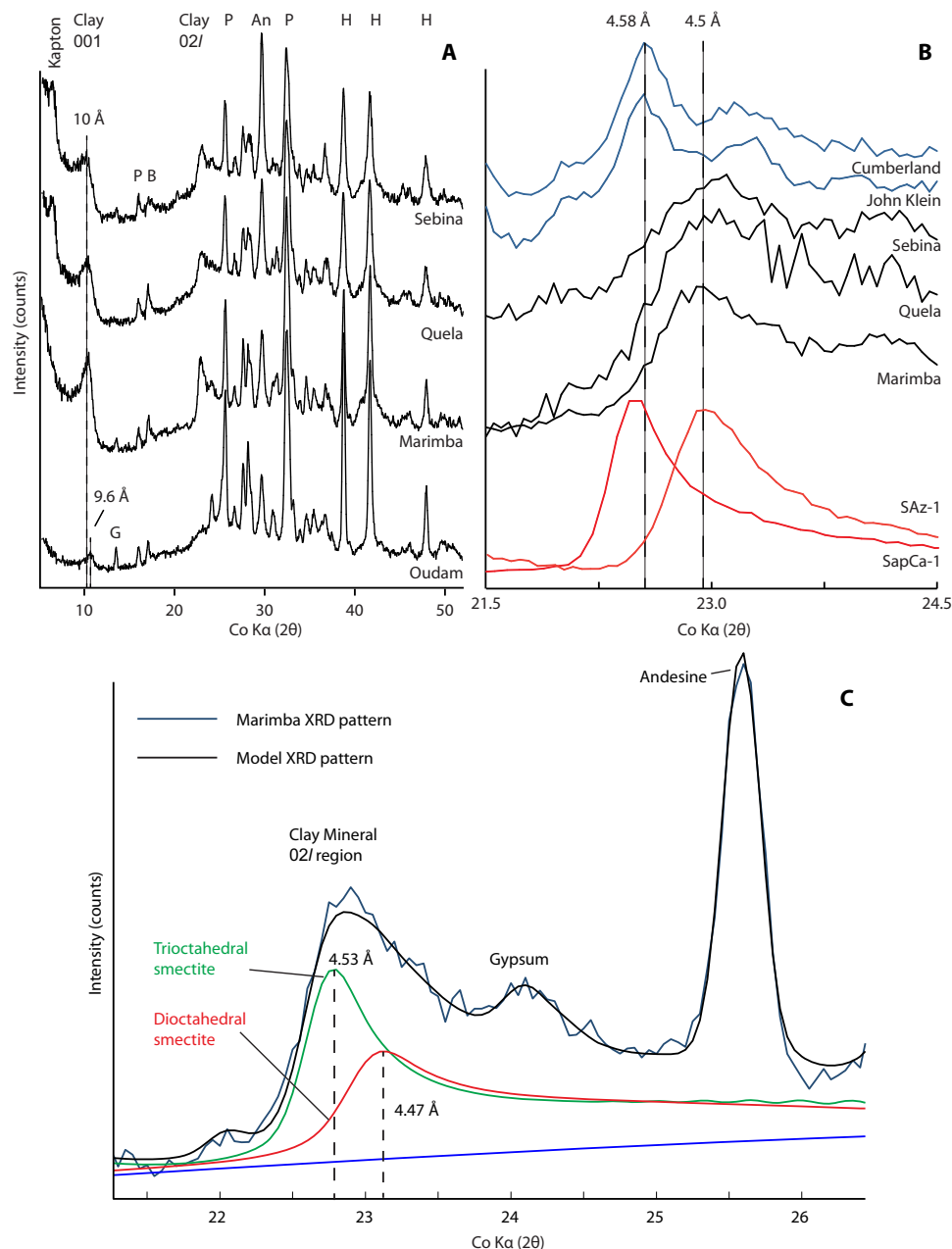


Fig. 3. XRD patterns of clay mineral-bearing sample from Gale crater. (A) Comparison of XRD patterns from Oudam, Marimba, Quela, and Sebina, with peaks assigned to clay minerals and other component minerals (A, anhydrite; B, bassanite; H, hematite; P, plagioclase). (B) Close-up comparison of Marimba, Quela, Sebina, and YKB XRD patterns with trioctahedral and dioctahedral smectite standards (SapCa-1 saponite and SAz-1 montmorillonite), showing the difference in 02/ band position corresponding to a difference in octahedral occupancy. (C) BGMN model of the 02/ band of Marimba showing contributions from trioctahedral and dioctahedral smectites.

Mg content in Murray saponite compared with YKB—a finding that is consistent with salinity-driven clay mineral formation mechanisms (28).

Although Oudam contains only ~3 wt % phyllosilicates, their basal (001) diffraction at ~9.6 Å is distinct from those of every other phyllosilicate-bearing sample measured by CheMin to date. Interlayer collapse to <10 Å, potentially induced by the dry air inside CheMin (4), is observed in certain smectites with small, monovalent cations, such as Na⁺, in the interlayer (32). However, we do not think that the ~9.6 Å peak in Oudam stems from collapsed smectite. Other smectite-bearing samples main-

tain basal spacings of ~10 Å inside CheMin, indicating the prevalence of bivalent interlayer cations (4). No evidence of a process leading to the preferential Na-exchange of Oudam clays is apparent from rover observations. Instead, Oudam siltstones appear to have been bathed in Ca²⁺-rich fluids, as shown by Ca-sulfate minerals in the matrix (Table 1).

A basal diffraction of ~9.6 Å is also characteristic of high-charge or zero-layer-charge phyllosilicates that lack interlayer H₂O, which include certain micas (for example, paragonite and margarite) and species in the pyrophyllite-talc series (for example, ferripyrophyllite).

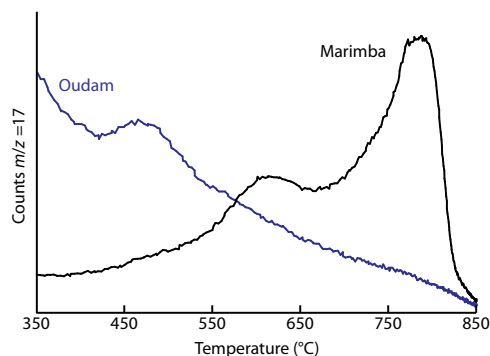


Fig. 4. SAM evolved H₂O release of Marimba and Oudam. Background has been subtracted from the EGA traces. The counts are not scaled.

The EGA trace for Oudam shows a single H₂O release at 470°C, which is reasonably attributable to dehydroxylation of a Fe(III)-rich phyllosilicate (21). Ferripyrophyllite is consistent with both XRD and EGA data (33). All of the candidate 9.6 Å phyllosilicate analogs recognized are the products of high-temperature hydrothermal and metamorphic processes. The absence of textural or mineralogical indicators of these processes at Oudam, and the presence of sedimentary structures indicative of an aeolian origin (14), leads us to hypothesize that Oudam phyllosilicates did not form in situ but are wind-blown detritus sourced elsewhere (29).

DISCUSSION

The contrast between the clay mineralogy of the Marimba, Quela, and Sebina mudstones with that of the 9.6 Å phyllosilicate in Oudam provides additional support linking smectite abundance and speciation with syn-depositional neof ormation and transformation processes rather than later period of genesis during burial diagenesis. We note that the Oudam sample has the same basic mineralogy as other Murray formation mudstones (Table 1), much of which could serve as precursors to smectite formation in an invasive diagenetic fluid model (26). In terrestrial sedimentary basins, the high porosity and permeability typical of sandstones promote more extensive production of burial diagenetic clay minerals compared with mudstones. On the basis of sedimentological observations, it appears that Oudam sediments spent less time in a dynamic aqueous environment close to the water table.

The discovery of a broad spectrum of mineralogical facies at Gale crater provides a window into the history of near-surface aqueous alteration processes on ancient Mars. On Earth, aqueous reactions at the juncture of the atmosphere, hydrosphere, and lithosphere (termed the critical zone) are central to biogeochemical cycles that regulate climate and biological productivity of the planet through the drawdown of greenhouse gases and release of nutrients (34). The unexpected abundance and diversity of clay minerals in sedimentary rocks at Gale crater and longevity of this sedimentary system (2) indicate near-surface aqueous alteration continued into the Early Hesperian on Mars. When integrated with sedimentological observations, clay mineral diversity provides additional insight into how environmental conditions evolved during and after the deposition of the strata of lower Aeolis Mons. Through the continued survey of sedimentary rocks at Gale, which are predicted to encompass a range of conditions, MSL has the opportunity to develop an understanding of how the martian critical zone operated and influenced planetary evolution.

MATERIALS AND METHODS

CheMin collects XRD data using Co radiation in transmission geometry [see the study of Blake *et al.* (35) for more details]. Curiosity's SA/SPaH system was used to drill Oudam, Marimba, Quela, and Sebina from the Murray formation bedrock (the majority of sample powder delivered to CheMin comes from a depth of 5 to 6 cm), sieve the resulting powder to <150 μm, and deliver ~50 mm³ of material to CheMin analysis cells, which have either Mylar or Kapton windows. Oudam and Marimba were delivered to Mylar cells, and Quela and Sebina were delivered to Kapton cells. Sample cells are reusable and located on a rotating sample wheel. The cells were shaken piezoelectrically during analysis to randomize grain orientations, presenting all lattice orientations to the incident Co x-rays. A charge-coupled device (CCD) detector was used to determine the energy and position of photons striking the CCD; fluoresced photons provided x-ray fluorescence (XRF) data, and the two-dimensional (2D) position of each diffracted Co K α photon was used to construct the diffraction pattern; circumferential integration of Debye diffraction rings, corrected for arc length, produced a conventional 1D XRD pattern with 2 θ resolution of ~0.3° (Fig. 3A). Positions of detected photons were summed over repeated 10-s measurements for several hours during each night of analysis. Samples were generally analyzed for four or more nights, spaced at time intervals determined by rover energy budget, allowance for operating other instruments, and other operational considerations. Plagioclase was a common phase in almost all samples, and the 1D diffraction patterns were corrected for minor variations in sample-to-detector distance using the best fit to plagioclase *c*- and γ -unit cell parameters (10). Abundances of crystalline phases in the Oudam, Marimba, Quela, and Sebina samples were determined by Rietveld analysis using Jade software. The mineral quantities presented in this paper (Table 1) differ slightly from results available in the Planetary Data System (PDS) (<https://pds.nasa.gov/>). These new results are products of Jade-based Rietveld refinements that incorporate clay mineral standard patterns in addition to structural models of crystalline phases. We found that this method improves model fits of measured XRD patterns.

The clay mineral standards used in these hybrid refinements were measured on CheMin 4—a prototype instrument that is similar to the CheMin flight instrument. We found that including both dioctahedral and trioctahedral smectite clay mineral standards led to the best replication of measured XRD patterns in Jade, consistent with our conclusion that Marimba, Quela, and Sebina contain both di- and trioctahedral smectite phases. Smectite clay mineral standards were heated to 200°C for 10 hours before analysis to remove interlayer H₂O and collapse basal spacing to ~10 Å, to more closely replicate the state of clay minerals within MSL. These approaches produced accurate identification and detection for virtually all crystalline phases at abundances greater than ~1 wt %. The abundances of amorphous components and poorly crystalline clay minerals were determined using the program FULLPAT (36) and remained as reported in the PDS.

The phases contributing to the pattern in the vicinity of the clay mineral 02l band were examined in more detail using BGMN, a Rietveld refinement program that can generate XRD patterns of partially disordered clay minerals and simultaneously consider contributions from crystalline phases (37, 38). BGMN uses instrument profiles as part of the XRD pattern modeling procedure. BGMN instrument profiles were generated based on description of the XRD instruments' geometry using ray-tracing simulations. BGMN's ray tracer does not support simulation of the flat CCD detector that collects CheMin patterns; therefore, we approximated profiles using a point detector, making adjustments to instrument geometry parameters until the profile function

reproduces unit cell parameters and peak shapes of the beryl standard that resides inside CheMin and was measured earlier in the mission.

BGMN refinements were used to estimate the relative proportions of dioctahedral and trioctahedral smectites in Marimba, Quela, and Sebina. These refinements include structural models of dehydrated dioctahedral smectite (based on montmorillonite) and a trioctahedral smectite (saponite). The *b*-unit cell parameter of the dioctahedral smectite phase was constrained to $<9 \text{ \AA}$ during refinements based on the relation between dehydroxylation temperature and Fe content of dioctahedral smectites in the study of Brigatti (25). Note that we report the ratios of dioctahedral/trioctahedral smectites from BGMN refinements because we do not have a reliable way to quantify the amount of x-ray amorphous material in our samples with BGMN.

To distinguish between illitic and smectitic clay minerals, we used potassium abundance data obtained by the APXS instrument onboard the Curiosity rover for Murray formation samples analyzed between sols 782 and 1496. These data are shown in table S1 with their reported analytical uncertainties. A complete description of the instrument, as well as the methods used for calibration and quantification of APXS data, can be found in the studies of Gellert *et al.* (39) and Campbell *et al.* (40). In summary, APXS is a contact instrument with Curium-244 sources that induce particle-induced x-ray emission and XRF to determine the abundance of major, minor, and trace elements from sodium to bromine in soil and rock targets. Low-atomic number (*Z*) element x-rays stemmed from the topmost 5 μm of the samples, and higher *Z* elements, like Fe, were detected from the upper $\sim 50 \mu\text{m}$. APXS is mounted on a turret at the end of the Curiosity rover's arm and was deployed on selected targets along the rover traverse to determine their elemental composition. The sampled area is about 1.7 cm in diameter when the instrument is in contact with the sample, and APXS spectra represent the average composition over the sampled area.

The SAM instrument suite consists of a quadrupole mass spectrometer (QMS), a six-column gas chromatograph, and a tunable laser spectrometer connected to a gas processing system that includes two pyrolysis ovens (24, 41, 42). Gases that evolved during pyrolysis of samples can be sent to several of these instruments; here, we focused on data from the direct QMS detection of gases during sample heating, referred to as EGA mass spectrometry. Volatiles that evolved during pyrolysis and their evolution temperatures can be used to inform the mineralogy or organic chemistry of samples. For further information about the SAM instrument and its operation, see the studies of Ming *et al.* (24), Mahaffy *et al.* (41), and Leshin *et al.* (42).

Splits of the $<150\text{-}\mu\text{m}$ portion of the Oudam and Marimba sample powders were delivered by SA/SPaH into cleaned (by heating to $>800^\circ\text{C}$) quartz sample cups. The mass of portions delivered to SAM cups was not measured in situ but was estimated to be $45 \pm 18 \text{ mg}$ (2σ) based on sample volume delivered during experiments with the Collection and Handling for Interior Martian Rock Analysis (CHIMRA) system test bed on Earth and analytical models (41, 42). Sample fines were then heated from $\sim 30^\circ\text{C}$ (ambient SAM temperature) to $\sim 860^\circ\text{C}$ at $35^\circ\text{C}/\text{min}$ under a helium carrier gas flow of ~ 0.8 standard cubic centimeters per minute and $\sim 25 \text{ mbar}$ of gas pressure in the sample pyrolysis ovens. A split of gases evolved from the sample during heating was swept into the QMS inlet and detected by the mass/charge ratio (*m/z*) of the molecules. If the main mass of a molecule saturated the MS detector, as was the case for *m/z* 18 from H_2O , then a signal for an isotopolog (for example, H_2^{18}O at *m/z* 20 for H_2O) or QMS fragment of the molecule (for example, *m/z* 17 for H_2O) was used to study the evolution of a molecule with temperature.

SUPPLEMENTARY MATERIALS

Supplementary material for this article is available at <http://advances.sciencemag.org/cgi/content/full/4/6/eaar3330/DC1>

table S1. Data used to infer the K content of clay minerals.

fig. S1. Comparison of the clay mineral and potassium content of Murray formation samples.

fig. S2. CRISM smectite signatures in the Murray formation (MF).

REFERENCES AND NOTES

1. J. P. Grotzinger, D. Y. Sumner, L. C. Kah, K. Stack, S. Gupta, L. Edgar, D. Rubin, K. Lewis, J. Schieber, N. Mangold, R. Milliken, P. G. Conrad, D. DesMarais, J. Farmer, K. Siebach, F. Calef III, J. Hurowitz, S. M. McLennan, D. Ming, D. Vaniman, J. Crisp, A. Vasavada, K. S. Edgett, M. Malin, D. Blake, R. Gellert, P. Mahaffy, R. C. Wiens, S. Maurice, J. A. Grant, S. Wilson, R. C. Anderson, L. Beegle, R. Arvidson, B. Hallet, R. S. Sletten, M. Rice, J. Bell III, J. Griffes, B. Ehlmann, R. B. Anderson, T. F. Bristow, W. E. Dietrich, G. Dromart, J. Eigenbrode, A. Fraeman, C. Hardgrove, K. Herkenhoff, L. Jandura, G. Kocurek, S. Lee, L. A. Leshin, R. Leveille, D. Limonadi, J. Maki, S. McCloskey, M. Meyer, M. Minitti, H. Newsom, D. Oehler, A. Okon, M. Palucis, T. Parker, S. Rowland, M. Schmidt, S. Squyres, A. Steele, E. Stolper, R. Summons, A. Treiman, R. Williams, A. Yingst, MSL Science Team, A habitable fluvio-lacustrine environment at Yellowknife Bay, Gale crater, Mars. *Science* **343**, 1242777 (2014).
2. J. P. Grotzinger, S. Gupta, M. C. Malin, D. M. Rubin, J. Schieber, K. Siebach, D. Y. Sumner, K. M. Stack, A. R. Vasavada, R. E. Arvidson, F. Calef III, L. Edgar, W. F. Fischer, J. A. Grant, J. Griffes, L. C. Kah, M. P. Lamb, K. W. Lewis, N. Mangold, M. E. Minitti, M. Palucis, M. Rice, R. M. E. Williams, R. A. Yingst, D. Blake, D. Blaney, P. Conrad, J. Crisp, W. E. Dietrich, G. Dromart, K. S. Edgett, R. C. Ewing, R. Gellert, J. A. Hurowitz, G. Kocurek, P. Mahaffy, M. J. McBride, S. M. McLennan, M. Mischna, D. Ming, R. Milliken, H. Newsom, D. Oehler, T. J. Parker, D. Vaniman, R. C. Wiens, S. A. Wilson, Deposition, exhumation, and paleoclimate of an ancient lake deposit, Gale crater, Mars. *Science* **350**, aac7575 (2015).
3. D. T. Vaniman, D. L. Bish, D. W. Ming, T. F. Bristow, R. V. Morris, D. F. Blake, S. J. Chipera, S. M. Morrison, A. H. Treiman, E. B. Rampe, M. Rice, C. N. Achilles, J. P. Grotzinger, S. M. McLennan, J. Williams, J. F. Bell III, H. E. Newsom, R. T. Downs, S. Maurice, P. Sarrazin, A. S. Yen, J. M. Morookian, J. D. Farmer, K. Stack, R. E. Milliken, B. L. Ehlmann, D. Y. Sumner, G. Berger, J. A. Crisp, J. A. Hurowitz, R. Anderson, D. J. Des Marais, E. M. Stolper, K. S. Edgett, S. Gupta, N. Spanovich, MSL Science Team, Mineralogy of a mudstone at Yellowknife Bay, Gale crater, Mars. *Science* **343**, 1243480 (2014).
4. T. F. Bristow, D. L. Bish, D. T. Vaniman, R. V. Morris, D. F. Blake, J. P. Grotzinger, E. B. Rampe, J. A. Crisp, C. N. Achilles, D. W. Ming, B. L. Ehlmann, P. L. King, J. C. Bridges, J. L. Eigenbrode, D. Y. Sumner, S. J. Chipera, J. Michael Moorokian, A. H. Treiman, S. M. Morrison, R. T. Downs, J. D. Farmer, D. Des Marais, P. Sarrazin, M. M. Floyd, M. A. Mischna, A. C. McAdam, The origin and implications of clay minerals from Yellowknife Bay, Gale crater, Mars. *Am. Mineral.* **100**, 824–836 (2015).
5. S. M. McLennan, R. B. Anderson, J. F. Bell III, J. C. Bridges, F. Calef III, J. L. Campbell, B. C. Clark, S. Clegg, P. Conrad, A. Cousin, D. J. Des Marais, G. Dromart, M. D. Dyar, L. A. Edgar, B. L. Ehlmann, C. Fabre, O. Forni, O. Gasnault, R. Gellert, S. Gordon, J. A. Grant, J. P. Grotzinger, S. Gupta, K. E. Herkenhoff, J. A. Hurowitz, P. L. King, S. Le Mouélac, L. A. Leshin, R. Leveille, K. W. Lewis, N. Mangold, S. Maurice, D. W. Ming, R. V. Morris, M. Nachon, H. E. Newsom, A. M. Ollila, G. M. Perrett, M. S. Rice, M. E. Schmidt, S. P. Schwenger, K. Stack, E. M. Stolper, D. Y. Sumner, A. H. Treiman, S. VanBommel, D. T. Vaniman, A. Vasavada, R. C. Wiens, R. A. Yingst, MSL Science Team, Elemental geochemistry of sedimentary rocks at Yellowknife Bay, Gale crater, Mars. *Science* **343**, 1244734 (2014).
6. P. R. Mahaffy, C. R. Webster, J. C. Stern, A. E. Brunner, S. K. Atreya, P. G. Conrad, S. Domagal-Goldman, J. L. Eigenbrode, G. J. Flesch, L. E. Christensen, H. B. Franz, C. Freissinet, D. P. Glavin, J. P. Grotzinger, J. H. Jones, L. A. Leshin, C. Malespin, A. C. McAdam, D. W. Ming, R. Navarro-Gonzalez, P. B. Niles, T. Owen, A. A. Pavlov, A. Steele, M. G. Trainer, K. H. Williford, J. J. Wray, MSL Science Team, The imprint of atmospheric evolution in the D/H of Hesperian clay minerals on Mars. *Science* **347**, 412–414 (2015).
7. E. B. Rampe, D. W. Ming, D. F. Blake, T. F. Bristow, S. J. Chipera, J. P. Grotzinger, R. V. Morris, S. M. Morrison, D. T. Vaniman, A. S. Yen, C. N. Achilles, P. I. Craig, D. J. Des Marais, R. T. Downs, J. D. Farmer, K. V. Fendrich, R. Gellert, R. M. Hazen, L. C. Kah, J. M. Morookian, T. S. Peretyazhko, P. Sarrazin, A. H. Treiman, J. A. Berger, J. Eigenbrode, A. G. Fairén, O. Forni, S. Gupta, J. A. Hurowitz, N. L. Lanza, M. E. Schmidt, K. Siebach, B. Sutter, L. M. Thompson, Mineralogical trends in mudstone deposits from the Murray formation, Gale crater, Mars. *Earth Planet. Sci. Lett.* **471**, 172–185 (2017).
8. J. A. Hurowitz, J. P. Grotzinger, W. W. Fischer, S. M. McLennan, R. E. Milliken, N. Stein, A. R. Vasavada, D. F. Blake, E. Dehouck, J. L. Eigenbrode, A. G. Fairén, J. Frydenvang, R. Gellert, J. A. Grant, S. Gupta, K. E. Herkenhoff, D. W. Ming, E. B. Rampe, M. E. Schmidt, K. L. Siebach, K. Stack-Morgan, D. Y. Sumner, R. C. Wiens, Redox stratification of an ancient lake in Gale crater, Mars. *Science* **356**, eaah6849 (2017).

9. A. H. Treiman, D. L. Bish, D. T. Vaniman, S. J. Chipera, D. F. Blake, D. W. Ming, R. V. Morris, T. F. Bristow, S. M. Morrison, M. B. Baker, E. B. Rampe, R. T. Downs, J. Filiberto, A. F. Glazner, R. Gellert, L. M. Thompson, M. E. Schmidt, L. Le Deit, R. C. Wiens, A. C. McAdam, C. N. Achilles, K. S. Edgett, J. D. Farmer, K. V. Fendrich, J. P. Grotzinger, S. Gupta, J. Michael Morookian, M. E. Newcombe, M. S. Rice, J. G. Spray, E. M. Stolper, D. Y. Sumner, A. R. Vasavada, A. S. Yen, Mineralogy, provenance, and diagenesis of a potassic basaltic sandstone on Mars: CheMin X-ray diffraction of the Windjana sample (Kimberley area, Gale Crater). *J. Geophys. Res. Planets* **121**, 75–106 (2016).
10. S. M. Morrison, R. T. Downs, D. F. Blake, D. T. Vaniman, D. W. Ming, E. B. Rampe, T. F. Bristow, C. N. Achilles, S. J. Chipera, A. S. Yen, R. V. Morris, A. H. Treiman, R. M. Hazen, P. C. Sarrazin, R. Gellert, K. V. Fendrich, J. M. Morookian, J. D. Farmer, D. J. Des Marais, P. I. Craig, Crystal chemistry of martian minerals from Bradbury Landing through Naukluff Plateau, Gale crater, Mars. *Am. Mineral.* **103**, 858–872 (2018).
11. C. E. Weaver, *Clays, Muds and Shales* (Elsevier, 1989), p. 819.
12. H. Chamley, *Clay Sedimentology* (Springer, 1989), p. 623.
13. A. Meunier, *Clays* (Springer, 2005), p. 472.
14. C. Fedo, J. Grotzinger, S. Gupta, N. T. Stein, J. Watkins, S. Banham, K. S. Edgett, M. Miniti, J. Schieber, K. Siebach, K. Stack-Morgan, H. Newsom, K. W. Lewis, C. House, A. R. Vasavada, Facies analysis and basin architecture of the upper part of the Murray formation, Gale crater, Mars (abstract 1689), in *48th Lunar and Planetary Science Conference*, The Woodlands, TX, 20 to 24 March 2017.
15. S. Gwizd, C. Fedo, J. Grotzinger, K. Edgett, F. Rivera-Hernandez, N. Stein, Depositional history of the Hartmann's Valley member, Murray formation, Gale crater, Mars (abstract 2150), in *48th Lunar and Planetary Science Conference*, The Woodlands, TX, 19 to 23 March 2018.
16. N. Stein, J. P. Grotzinger, J. Schieber, N. Mangold, H. Newsom, M. Miniti, D. Sumner, K. S. Edgett, K. Stack, C. Fedo, S. Gupta, B. Hallet, A. Vasavada, D. Fey, Candidate desiccation cracks in the upper Murray formation, Gale crater, Mars (abstract 2387), in *48th Lunar and Planetary Science Conference*, The Woodlands, TX, 21 March 2017.
17. B. L. Ehlmann, J. F. Mustard, S. L. Murchie, Jean-Pierre Bibring, Alain Meunier, Abigail A. Fraeman, Yves Langevin, Subsurface water and clay mineral formation during the early history of Mars. *Nature* **479**, 53–60 (2011).
18. J. Carter, F. Poulet, J.-P. Bibring, N. Mangold, S. L. Murchie, Hydrous minerals on Mars as seen by the CRISM and OMEGA imaging spectrometers: Updated global view. *J. Geophys. Res. Planets* **118**, 831–858 (2013).
19. J. R. Michalski, J. Cuadros, J. L. Bishop, M. D. Dyar, V. Dekov, S. Fiore, Constraints on the crystal-chemistry of Fe/Mg-rich smectitic clays on Mars and links to global alteration trends. *Earth Planet. Sci. Lett.* **427**, 215–225 (2015).
20. D. M. Moore, R. C. Reynolds Jr., *X-ray Diffraction and the Identification and Analysis of Clay Minerals* (Oxford Univ. Press, 1997), p. 382.
21. L. Heller-Kallai, I. Rozenon, Dehydroxylation of dioctahedral phyllosilicates. *Clays Clay Miner.* **28**, 355–368 (1980).
22. A. Derkowski, V. A. Drits, D. K. McCarty, Nature of rehydroxylation in dioctahedral 2:1 layer clay minerals. *Am. Mineral.* **97**, 610–629 (2012).
23. J. Cuadros, J. R. Michalski, V. Dekov, J. L. Bishop, S. Fiore, M. D. Dyar, Crystal-chemistry of interstratified Mg/Fe-clay minerals from seafloor hydrothermal sites. *Chem. Geol.* **360–361**, 142–158 (2013).
24. D. W. Ming, P. D. Archer Jr., D. P. Glavin, J. L. Eigenbrode, H. B. Franz, B. Sutter, A. E. Brunner, J. C. Stern, C. Freissinet, A. C. McAdam, P. R. Mahaffy, M. Cabane, P. Coll, J. L. Campbell, S. K. Atreya, P. B. Niles, J. F. Bell III, D. L. Bish, W. B. Brinckerhoff, A. Buch, P. G. Conrad, D. J. Des Marais, B. L. Ehlmann, A. G. Fairén, K. Farley, G. J. Flesch, P. Francois, R. Gellert, J. A. Grant, J. P. Grotzinger, S. Gupta, K. E. Herkenhoff, J. A. Hurowitz, L. A. Leshin, K. W. Lewis, S. M. McLennan, K. E. Miller, J. Moersch, R. V. Morris, R. Navarro-González, A. A. Pavlov, G. M. Perrett, I. Pradler, S. W. Squyres, R. E. Summons, A. Steele, E. M. Stolper, D. Y. Sumner, C. Szopa, S. Teinturier, M. G. Trainer, A. H. Treiman, D. T. Vaniman, A. R. Vasavada, C. R. Webster, J. J. Wray, R. A. Yingst, MSL Science Team, Volatile and organic compositions of sedimentary rocks in Yellowknife Bay Gale crater, Mars. *Science* **343**, 1245267 (2014).
25. M. F. Brigatti, Relationships between composition and structure in Fe-rich smectites. *Clay Miner.* **18**, 177–186 (1983).
26. A. A. Fraeman, B. L. Ehlmann, R. E. Arvidson, C. S. Edwards, J. P. Grotzinger, R. E. Milliken, D. P. Quinn, M. S. Rice, The stratigraphy and evolution of lower Mount Sharp from spectral, morphological, and thermophysical orbital data sets. *J. Geophys. Res. Planets* **1713–1736** (2016).
27. J. Carter, B. Gondet, Y. Langevin, MSL Homing in on a large smectite clay deposit: An orbital perspective (abstract 1899), in *47th Lunar and Planetary Science Conference*, The Woodlands, TX, 22 March 2016.
28. T. F. Bristow, R. E. Milliken, Terrestrial perspective on authigenic clay mineral production in ancient martian lakes. *Clays Clay Miner.* **59**, 339–358 (2011).
29. J. Buz, B. L. Ehlmann, L. Pan, J. P. Grotzinger, Mineralogy and stratigraphy of the Gale crater rim, wall, and floor units. *J. Geophys. Res. Planets* **122**, 1090–1118 (2017).
30. N. M. Mangold, E. Dehouck, O. Forni, C. Fedo, C. Achilles, T. Bristow, J. Frydevang, O. Gasnault, J. L'Haridon, L. Le Deit, S. Maurice, S.M. McLennan, P. Y. Meslin, S. Morrison, H. E. Newsom, E. Rampe, F. Rivera-Hernandez, M. Salvatore, R. C. Wiens, Open-system weathering at Gale crater from the chemistry of mudstones analyzed by the Curiosity rover (abstract 3013), in *Fourth International Conference on Early Mars*, Flagstaff, AZ, 2 to 6 October 2017.
31. V. C. Hover, L. M. Walter, D. R. Peacor, A. M. Martini, Mg-smectite authigenesis in a marine evaporative environment, Salina Ometepe, Baja California. *Clays Clay Miner.* **47**, 252–268 (1999).
32. T. Sato, T. Watanabe, R. Otsuka, Effects of layer charge, charge location, and energy change on expansion properties of dioctahedral smectites. *Clays Clay Miner.*, **40**, 103–113 (1992).
33. F. V. Chukhrov, B. B. Zvyagin, V. A. Drits, A. I. Gorshkov, L. P. Ermilova, E. A. Goilo, E. S. Rudnitskaya, The ferric analogue of pyrophyllite and related phases. Proceedings of the International Clay Conference 1978, in *Developments in Sedimentology* (Elsevier, 1979), pp. 55–64.
34. R. Amundson, D. D. Richter, G. S. Humphreys, E. G. Jobbágy, J. Gaillardet, Coupling between biota and Earth materials in the Critical Zone. *Elements* **3**, 327–332 (2007).
35. D. F. Blake, D. Vaniman, C. Achilles, R. Anderson, D. Bish, T. Bristow, C. Chen, S. Chipera, J. Crisp, D. Des Marais, R. T. Downs, J. Farmer, S. Feldman, M. Fonda, M. Gaillanhou, H. Ma, D. W. Ming, R. V. Morris, P. Sarrazin, E. Stolper, A. Treiman, A. Yen, Characterization and calibration of the CheMin mineralogical instrument on Mars Science Laboratory. *Space Sci. Rev.* **170**, 341–399 (2012).
36. S. J. Chipera, D. L. Bish, FULLPAT: A full-pattern quantitative analysis program for X-ray powder diffraction using measured and calculated patterns. *J. Appl. Crystallogr.* **35**, 744–749 (2002).
37. J. Bergmann, P. Friedel, R. Kleeberg, BGMN—A new fundamental parameter-based Rietveld program for laboratory X-ray sources, its use in quantitative analysis and structure investigations. *CPD Newsletter* **20**, 5–8 (1998).
38. K. Ufer, G. Roth, R. Kleeberg, H. Stanjek, R. Dohrmann, J. Bergmann, Description of X-ray powder pattern of turbostratically disordered layer structures with a Rietveld compatible approach. *Z. Kristallogr.*, **219**, 519–527 (2004).
39. R. Gellert, R. Rieder, J. Brückner, B. C. Clark, G. Dreibus, G. Klingelhofer, G. Lugmair, D. W. Ming, H. Wänke, A. Yen, J. Zipfel, S. W. Squyres, The Alpha Particle X-Ray Spectrometer (APXS): Results from Gusev Crater and calibration report. *J. Geophys. Res.* **111**, E02S05 (2006).
40. J. L. Campbell, G. M. Perrett, R. Gellert, S. M. Andrushenko, N. I. Boyd, J. A. Maxwell, P. L. King, C. D. M. Schofield, Calibration of the Mars Science Laboratory alpha particle X-ray spectrometer. *Space Sci. Rev.* **170**, 319–340 (2012).
41. P. R. Mahaffy, C. R. Webster, M. Cabane, P. G. Conrad, P. Coll, S. K. Atreya, R. Arvey, M. Barciniak, M. Benna, L. Bleacher, W. B. Brinckerhoff, J. L. Eigenbrode, D. Carignan, M. Cascia, R. A. Chalmers, J. P. Dworkin, T. M. Davison, P. Everson, H. Franz, R. Farley, S. Feng, G. Frazier, C. Freissinet, D. P. Glavin, D. N. Harpold, D. Hawk, V. Holmes, C. S. Johnson, A. Jones, P. Jordan, J. Kellogg, J. Lewis, E. Lyness, C. A. Malespin, D. K. Martin, J. Maurer, A. C. McAdam, D. McLennan, T. J. Nolan, M. Noriega, A. A. Pavlov, B. Prats, E. Raean, O. Sheinman, D. Sheppard, J. Smith, J. C. Stern, F. Tan, M. Trainer, D. W. Ming, R. V. Morris, J. Jones, C. Gundersen, A. Steele, J. Wray, O. Botta, L. A. Leshin, T. Owen, S. Battel, B. M. Jakosky, H. Manning, S. Squyres, R. Navarro-González, C. P. McKay, F. Raulin, R. Sternberg, A. Buch, P. Sorensen, R. Kline-Schoder, D. Coscia, C. Szopa, S. Teinturier, C. Baffes, J. Feldman, G. Flesch, S. Forouhar, R. Garcia, D. Keymeulen, S. Woodward, B. P. Block, K. Arnett, R. Miller, C. Edmonson, S. Gorevan, E. Mumm, The sample analysis at Mars investigation and instrument suite. *Space Sci. Rev.* **170**, 401–478 (2012).
42. L. A. Leshin, P. R. Mahaffy, C. R. Webster, M. Cabane, P. Coll, P. G. Conrad, P. D. Archer Jr., S. K. Atreya, A. E. Brunner, A. Buch, J. L. Eigenbrode, G. J. Flesch, H. B. Franz, C. Freissinet, D. P. Glavin, A. C. McAdam, K. E. Miller, D. W. Ming, R. V. Morris, R. Navarro-González, P. B. Niles, T. Owen, R. O. Pepin, S. Squyres, A. Steele, J. C. Stern, R. E. Summons, D. Y. Sumner, B. Sutter, C. Szopa, S. Teinturier, M. G. Trainer, J. J. Wray, J. P. Grotzinger, MSL Science Team, Volatile, isotope, and organic analysis of martian fines with the Mars Curiosity rover. *Science* **341**, 1238937 (2013).

Acknowledgments: We are grateful to R. Kleeberg who helped develop the CheMin instrument profile model for BGMN and A. Derkowski for informative discussion. S. Hillier and J. Michalski are thanked for constructive reviews. We acknowledge the support of the Jet Propulsion Laboratory engineering and management teams, and MSL science team members who participated in tactical and strategic operations, without whom the data presented here could not have been collected. Some of this research was carried out at the Jet Propulsion Laboratory, California Institute of Technology, under a contract with NASA.

Funding: S.G. acknowledges funding from the UK Space Agency (UKSA) (grants ST/J005169/1 and ST/N000579/1). N.M. is funded by the Centre National d'Etudes Spatial (CNES). A.C.M. and B.H. thank NASA's MSL Participating Scientist program for supporting this effort. **Author contributions:** T.F.B. wrote the manuscript, with corrections, discussions, and/or revised text from coauthors. D.F.B., J.A.C., R.G., J.P.G., P.R.M., D.T.V., and A.R.V. were key in designing instruments and guiding the mission. All authors analyzed data and performed operational roles in data collection. **Competing interests:** The authors declare that they have no competing interests. **Data and materials availability:** All data discussed in this manuscript are available from the PDS (<https://pds.nasa.gov/>) and the CheMin Database (<http://odr.io/CheMin>). Files and models required to replicate XRD refinements are available upon request.

Submitted 26 October 2017

Accepted 24 April 2018

Published 6 June 2018

10.1126/sciadv.aar3330

Citation: T. F. Bristow, E. B. Rampe, C. N. Achilles, D. F. Blake, S. J. Chipera, P. Craig, J. A. Crisp, D. J. Des Marais, R. T. Downs, R. Gellert, J. P. Grotzinger, S. Gupta, R. M. Hazen, B. Horgan, J. V. Hogancamp, N. Mangold, P. R. Mahaffy, A. C. McAdam, D. W. Ming, J. M. Morookian, R. V. Morris, S. M. Morrison, A. H. Treiman, D. T. Vaniman, A. R. Vasavada, A. S. Yen, Clay mineral diversity and abundance in sedimentary rocks of Gale crater, Mars. *Sci. Adv.* **4**, eaar3330 (2018).

Clay mineral diversity and abundance in sedimentary rocks of Gale crater, Mars

Thomas F. Bristow, Elizabeth B. Rampe, Cherie N. Achilles, David F. Blake, Steve J. Chipera, Patricia Craig, Joy A. Crisp, David J. Des Marais, Robert T. Downs, Ralf Gellert, John P. Grotzinger, Sanjeev Gupta, Robert M. Hazen, Briony Horgan, Joanna V. Hogancamp, Nicolas Mangold, Paul R. Mahaffy, Amy C. McAdam, Doug W. Ming, John Michael Morookian, Richard V. Morris, Shauna M. Morrison, Allan H. Treiman, David T. Vaniman, Ashwin R. Vasavada and Albert S. Yen

Sci Adv 4 (6), eaar3330.
DOI: 10.1126/sciadv.aar3330

ARTICLE TOOLS

<http://advances.sciencemag.org/content/4/6/eaar3330>

SUPPLEMENTARY MATERIALS

<http://advances.sciencemag.org/content/suppl/2018/06/04/4.6.eaar3330.DC1>

REFERENCES

This article cites 30 articles, 15 of which you can access for free
<http://advances.sciencemag.org/content/4/6/eaar3330#BIBL>

PERMISSIONS

<http://www.sciencemag.org/help/reprints-and-permissions>

Use of this article is subject to the [Terms of Service](#)